

The anomalous production of multi-leptons and its impact on the measurement of Wh production at the LHC

Yesenia Hernandez^{a,1}, Mukesh Kumar^{b,1}, Alan S. Cornell^{c,2}, Salah-Eddine Dahbi^{d,1}, Yaquan Fang^{e,3,4}, Benjamin Lieberman^{f,1}, Bruce Mellado^{g,1,5}, Kgomotso Monnakgotla^{h,1}, Xifeng Ruan^{i,1}, Shuiting Xin^{j,3,4}

¹School of Physics and Institute for Collider Particle Physics, University of the Witwatersrand, Johannesburg, Wits 2050, South Africa.

²Department of Physics, University of Johannesburg, PO Box 524, Auckland Park 2006, South Africa.

³Institute of High Energy Physics, 19B, Yuquan Road, Shijing District, Beijing, China, 100049.

⁴University of Chinese Academy of Sciences (CAS), 19A Yuquan Road, Shijing District, Beijing, China, 100049.

⁵iThemba LABS, National Research Foundation, PO Box 722, Somerset West 7129, South Africa.

Received: date / Accepted: date

Abstract Anomalies in multi-lepton final states at the Large Hadron Collider (LHC) have been reported in Refs. [1, 2]. These can be interpreted in terms of the production of a heavy boson, H , decaying into a Standard Model (SM) Higgs boson, h , and a singlet scalar, S , which is treated as a SM Higgs-like boson. This process would naturally affect the measurement of the Wh signal strength at the LHC, where h is produced in association with leptons and di-jets. Here, h would be produced with lower transverse momentum, p_{T_h} , compared to SM processes. Corners of the phase-space are fixed according to the model parameters derived in Refs. [1, 3] without additional tuning, thus nullifying potential look-else-where effects or selection biases. Provided that no stringent requirements are made on p_{T_h} or related observables, the signal strength of Wh is $\mu(Wh) = 2.41 \pm 0.37$. This corresponds to a deviation from the SM of 3.8σ . This result further strengthens the need to measure with precision the SM Higgs boson couplings in e^+e^- , and e^-p collisions, in addition to pp collisions.

1 Introduction

The discovery of a Higgs boson (h) [4–7] at the Large Hadron Collider (LHC) by the ATLAS [8] and CMS [9] experiments has opened a new chapter in particle physics. Measurements

provided so far indicate that the quantum numbers of this boson are consistent with those predicted by the Standard Model (SM) [10, 11], and that the relative branching ratios (BRs) to SM particles follow what is predicted by the SM. With this in mind, a window of opportunity now opens for the search for new bosons and how these would affect the h boson measurements.

One of the implications of a 2HDM+S model, where S is a scalar SM singlet, is the production of multiple-leptons through the decay chain $H \rightarrow Sh, SS$ [3], where H is the heavy CP-even scalar and h is the SM Higgs boson. Excesses in multi-lepton final states were reported in Ref. [1]. In order to further explore results with more data and new final states while avoiding biases and look-else-where effects, the parameters of the model were fixed in 2017 according to Refs. [1, 3]. This includes setting the scalar masses as $m_H = 270$ GeV, $m_S = 150$ GeV, treating S as a SM Higgs-like scalar and assuming the dominance of the decays $H \rightarrow Sh, SS$. Excesses in opposite sign di-leptons, same-sign di-leptons, and three leptons, with and without the presence of b -tagged hadronic jets were reported in Ref. [2].

In Ref. [12] the impact on the measurement of the process $H \rightarrow Sh$ was evaluated in final states including $h \rightarrow \gamma\gamma$ in association with hadronic jets. In particular, it was demonstrated that the impact on the measurement of h produced via vector boson fusion (VBF) would be moderate, where the measurement of h in association with $W \rightarrow jj$ would be affected significantly, as long as the transverse momentum of h , $p_{T_h} < m_W$, where m_W is the mass of the W boson.

In this article we expand on Ref. [12] by studying the potential impact on measurements related to $Wh, W \rightarrow jj/\ell\nu$ ($\ell = e, \mu$) and other relevant final states used in the measurement of the signal strength of Wh by the LHC experiments. A survey of the existing measurements of the cross-section of the Wh production mechanism from the ATLAS and CMS

^ae-mail: yesenia@cern.ch

^be-mail: mukesh.kumar@cern.ch

^ce-mail: acornell@uj.ac.za

^de-mail: salah-eddine.dahbi@cern.ch

^ee-mail: fangyq@ihep.ac.cn

^fe-mail: benjamin.lieberman@cern.ch

^ge-mail: bmellado@mail.cern.ch

^he-mail: jeremiah.kgomotso.monnakgotla@cern.ch

ⁱe-mail: xifeng.ruan@cern.ch

^je-mail: shuiting.xin@cern.ch

experiments is performed, with emphasis on measurements of the signal strength of the Wh production mechanism in the corner of the phase-space where $p_{Th} < m_W$ is explored. Here we evaluate the size of the deviation from the SM in the production of Wh , as measured by the LHC experiments. The final states considered here were not included in the statistical analyses reported in Refs. [1, 2].

The paper is organised as follows: Section 2 succinctly describes the simplified model used to model the BSM signal described above; Section 3 reports on the available data and the methodology used to study it; Section 4 points to the compatibility of the results with the measurements of inclusive observables made by the experiments; Section 5 summarises the findings of the paper and quantifies the size of the observed anomaly in the Higgs boson data.

2 The Simplified Model

In the model, the scalar H has Yukawa couplings as it is assumed to be related to EW symmetry breaking (EWSB). The simplified Lagrangian used to describe the production of H is:

$$\mathcal{L}_H = -\frac{1}{4} \beta_g \kappa_{hgg}^{\text{SM}} G_{\mu\nu} G^{\mu\nu} H + \beta_V \kappa_{hVV}^{\text{SM}} V_\mu V^\mu H. \quad (1)$$

These are the effective vertices required so that H couples to gluons and the heavy vector bosons $V = W^\pm, Z$, respectively. The first term in 1 allows for the gluon fusion (ggF) production mode of H , while the second term describes the VBF production mode of H and VH production mode. The κ_{hgg}^{SM} and κ_{hVV}^{SM} are the effective coefficients for the equivalent SM Higgs gluon fusion, and Higgs vector-boson fusion, whilst $\beta_g = y_{tH}/y_{tth}$ is the scale factor with respect to the SM top-Yukawa coupling for H . Therefore, it is used for tuning the effective ggF coupling. Similarly, β_V represents the scale factor used to tune the VVH couplings.

On the other hand, the S boson is assumed to only be produced through the H decay so that its direct production is suppressed. The S boson is included in this model as a singlet scalar that interacts with H and the SM Higgs boson h . This allows the H particle to produce S bosons through the $H \rightarrow SS$ and Sh decay modes. The assumption here considers the $H \rightarrow Sh$ decay mode to have a 100% BR. The effective interaction Lagrangians described in the following consider all these assumptions. The S boson couples to the scalar sector as below:

$$\mathcal{L}_{HhS} = -\frac{1}{2} v \left[\lambda_{hhs} hhS + \lambda_{hSS} hSS + \lambda_{HHS} HHS + \lambda_{HSS} HSS + \lambda_{HhS} HhS \right], \quad (2)$$

where the couplings are fixed to ensure that the BR for the $H \rightarrow Sh$ must satisfy the constraints discussed in [13]. Furthermore, by fixing the parameters in the Lagrangian BRs of

the Higgs-like S boson are achieved. The effective interactions can be written as:

$$\begin{aligned} \mathcal{L}_S = & \frac{1}{4} \kappa_{Sgg} \frac{\alpha_s}{12\pi v} S G^{a\mu\nu} G_{\mu\nu}^a + \frac{1}{4} \kappa_{S\gamma\gamma} \frac{\alpha}{\pi v} S F^{\mu\nu} F_{\mu\nu} \\ & + \frac{1}{4} \kappa_{SZ\gamma} \frac{\alpha}{\pi v} S Z^{\mu\nu} F_{\mu\nu} + \kappa_{SZZ} m_Z S Z Z \\ & + \kappa_{Sww} m_W S W^+ W^- - \sum_f \kappa_{Sff} \frac{m_f}{v} S \bar{f} f. \end{aligned} \quad (3)$$

Additionally, the couplings are globally re-scaled in order to suppress the direct production of S .

In the model the number of free parameters is reduced by fixing the BRs of S . For simplicity the BRs of S are set to the same as that of a SM Higgs boson in the mass range considered here. In the above Lagrangian, $Z_{\mu\nu} = D_\mu Z_\nu - D_\nu Z_\mu$, $F_{\mu\nu}$ is the usual electromagnetic field strength tensor and f refers to the SM fermions. Here, we neglect other possible terms for the self interaction of S as they are not phenomenologically interesting for this study.

It is also important to mention that the Lagrangians used here are the subset of full 2HDM+S models [3, 13, 14], where the couplings associated with particle spectrum of the model are functions of appropriate mixing angles of three CP-even scalars (h, H, S), a CP-odd scalar (A) and charged scalar (H^\pm). The parameters in Ref. [13] also satisfy the: (a) theoretical constraints, like tree-level perturbative unitarity, the vacuum stability from global minimum conditions of the 2HDM+S potential and conditions which bound the potential from below; (b) the experimental constraints from $B \rightarrow X_s \gamma$ and R_b ; and (c) the compatibility with the oblique parameters S, T and U .

3 Methodology

The analyses for the associated production of h with a W or Z bosons through Drell-Yan processes typically exploit the feature that h is produced with larger transverse momentum than the SM background processes. The SM Vh signal sensitivity is enhanced by considering corners of the phase-space with $p_{Th} > m_W$ where backgrounds can be strongly suppressed. This is actively used by the LHC experiments to effectively extract the h signal for measurements of the signal strength. This implies that searches and measurements of Wh at the LHC favor regions of the phase-space with $p_{Th} > m_W$ where a significantly large rate of h can be produced. The high p_{Th} restriction has to be taken into account if one is looking for deviations from the SM in the Higgs sector. This is achieved either by truncating the phase-space, excluding low p_{Th} with large backgrounds, or by implementing multivariate analyses that include observables sensitive to p_{Th} , where the relative weight of large transverse momentum production is enhanced.

By contrast, with the BSM signal $H \rightarrow Sh$ with $m_H = 270$ GeV, $m_S = 150$ GeV and $m_h = 125$ GeV, h displays significantly lower transverse momentum [3]. To a considerable degree, the h signal produced via SM and BSM production mechanisms appears adjacent, but are distinct regions of the phase-space. The results provided by the ATLAS and CMS experiments pertain to the search and measurement of Wh production in the SM and are not optimal for the search for new physics in general, and the BSM signal considered here, in particular. Nonetheless, a straw man approach is adopted here, whereby results that rely heavily on p_{Th} , or correlated observables, are discarded. Those results that explore the phase-space more “inclusively” are considered here instead.

It is important to reiterate that all considerations related to choice of phase-space or whether an analysis is discarded or not are based on a model with fixed parameters, as detailed in Ref [1, 3] and dating back to 2017. This includes the above mentioned scalar masses, securing the dominance of the $H \rightarrow Sh$ decay and considering S as a SM Higgs-like scalar. This is a concerted effort in order not to scan of the phase-space, thus nullifying the potential biases or look-else-where effects.

Table 1 summarises the results from ATLAS and CMS experiments for the SM Higgs boson produced to date in association with a W boson in leptonic and di-jet final states. The reported signal strength (μ) is provided by the respective publications. The Higgs decay modes considered here include $h \rightarrow WW, ZZ, \tau\tau$ and $\gamma\gamma$. Results from the $h \rightarrow b\bar{b}$ decay mode are not considered here as these analyses focus on large transverse momentum of the vector boson [15, 16]. In the following the main event selection for each analysis is briefly described and the motivation for including the results in Section 5 is discussed. The results included in the combination are selected by comparing the key kinematic distributions used in each analysis for the $H \rightarrow Sh$ and SM Wh processes from Monte Carlo simulation. Simulated events are generated with PYTHIA8 [17] using the NNPDF 2.3 LO [18] for parton showering, with the A14 tune [19], and without considering detector effects.

While the parameters of the model are fixed, we also present the kinematics of the final state with $m_H = 250$ GeV and $m_H = 260$ GeV, in addition to the nominal value. The $H \rightarrow Sh$ samples are generated including $WW, ZZ, \tau\tau$ and $\gamma\gamma$ decay modes for the S and h bosons to obtain the relevant final states with leptons, photons and jets for this study. Finally, the SM Vh events are generated for each Higgs boson decay mode of interest separately.

3.1 $Vh \rightarrow VWW$

The Wh results in the $h \rightarrow WW^*$ decay using the Run 1 data sample collected at the ATLAS detector are obtained in two-

and three-lepton final states [20], denoted in the following as 2ℓ and 3ℓ , respectively. The former requires exactly two well isolated leptons with high transverse momentum and is further split in different-flavour opposite-sign (DFOS) and same-sign (SS) 2ℓ channels.

In the DFOS 2ℓ category the vector boson (either a W or Z boson) associated to the Higgs boson decays hadronically and produces two jets, while the $e^\pm\mu^\mp$ pair originates from the $h \rightarrow WW^*$ process. The SS 2ℓ channel targets Wh production when the W boson that radiates the Higgs boson decays leptonically, while one of the W bosons coming from $h \rightarrow WW^*$ decays hadronically, and the other - with same charge as the former W boson - decays leptonically. In both categories lower bounds on the invariant mass of the lepton pair ($m_{\ell\ell}$) and on the missing transverse energy (E_T^{miss}) are applied, as well as a veto on events with the presence of b -tagged jets. For DFOS 2ℓ events, several constraints on the dijet kinematics are required to select jets associated to W/Z bosons. The rapidity separation between the two highest p_T jets, $\Delta y_{jj} < 1.2$, and the invariant mass of these two jets, $|m_{jj} - 85| < 15$ GeV, are imposed. Finally, the selection exploits the kinematics of the lepton pair to be consistent with the $h \rightarrow WW^*$ decay, so the azimuthal angular separation between the two leptons ($\Delta\phi_{\ell\ell}$) is required to be below 1.8 rad and $m_{\ell\ell} < 50$ GeV. In the SS 2ℓ channel a further categorisation divides the events by having exactly one jet or exactly two jets in the final state. Similarly to the DFOS category, a set of requirements on the minimum invariant mass of a lepton and a jet, the smallest opening angle between the lepton which minimises the above variable and a jet, and the transverse mass of the leading lepton and the E_T^{miss} (m_T) are used. All these channels present an observed signal strength which is above the unity by one to two standard deviations (σ), as observed in Table 1. The measured signal strength of the 2ℓ categories in ATLAS using Run 1 data results in $3.7_{-1.5}^{+1.9}$ [20]. This result will be used in this paper.

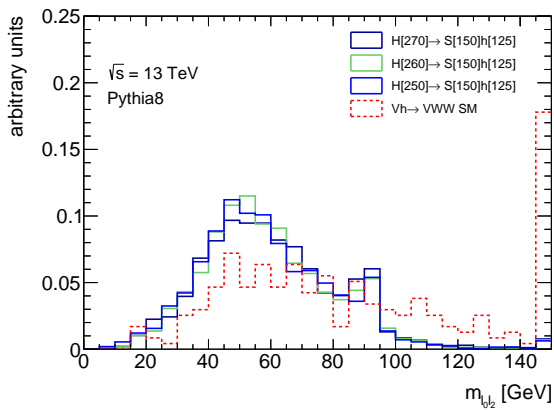
In the 3ℓ channel the W bosons are expected to decay leptonically. These events are selected by having exactly three leptons with total charge of ± 1 and at most one jet in the final state. Events are further categorised depending on the presence of same-flavour opposite-sign (SFOS) lepton pairs: 0SFOS and 1SFOS. The 0SFOS category includes $e^\pm e^\pm \mu^\mp$ and $\mu^\pm \mu^\pm e^\mp$ final states. These types of events highly benefit from low background contamination and no additional selection is applied. The angular separation of the Higgs decay lepton candidates ($\Delta R_{\ell\ell}$) is used in the likelihood fit to extract the results. The observed signal strength of the 0SFOS category is $1.7_{-1.4}^{+1.9}$ and it will be considered in the results section. Events with at least 1SFOS lepton pair require $\Delta R_{\ell\ell} < 2$ and the invariant mass of all SFOS combinations must satisfy $|m_{\ell^\pm \ell^\mp} - m_Z| > 25$ GeV in order to reject WZ and ZZ events. In addition, a multivariate discriminant based on Boosted Decision Trees (BDT) [34, 35]

Higgs decay	Ref.	Experiment	\sqrt{s}, \mathcal{L} TeV, fb ⁻¹	Final state	Category	μ	Used in combination	Comments
WW	[20]	ATLAS	7, 4.5 8, 20.3	2 ℓ	DFOS 2j	$2.2^{+2.0}_{-1.9}$	✓(Vh)	2 ℓ combination: $\mu = 3.7^{+1.9}_{-1.5}$ $m_{\ell_0\ell_2}$ used as input BDT discriminating variable
					SS 1j	$8.4^{+4.3}_{-3.8}$	✓(Vh)	
					SS 2j	$7.6^{+6.0}_{-5.4}$	✓(Vh)	
					1SFOS	$-2.9^{+2.7}_{-2.1}$	x	
					0SFOS	$1.7^{+1.9}_{-1.4}$	✓(Wh)	
	[21]	ATLAS	13, 36.1	3 ℓ	1SFOS 0SFOS	$2.3^{+1.2}_{-1.0}$	✓(Wh)	1SFOS channel uses $m_{\ell_0\ell_2}$ in the BDT but excess driven by 0SFOS
	[22]	CMS	7, 4.9 8, 19.4	2 ℓ	DFOS 2j	$0.39^{+1.97}_{-1.87}$	✓(Vh)	Discrepancy at low $m_{\ell\ell}$
	3 ℓ			0+1SFOS	$0.56^{+1.27}_{-0.95}$	✓(Wh)		
	[23]	CMS	13, 35.9	2 ℓ	DFOS 2j	$3.92^{+1.32}_{-1.17}$	✓(Vh)	Discrepancy at low $m_{\ell\ell}$
	3 ℓ			0+1SFOS	$2.23^{+1.76}_{-1.53}$	✓(Wh)		
$\tau\tau$	[24]	ATLAS	8, 20.3	1 ℓ 2 ℓ	$\ell + \tau_h \tau_h$ $e^\pm \mu^\pm + \tau_h$	1.8 ± 3.1 1.3 ± 2.8	✓(Wh) ✓(Wh)	
	[25]	CMS	7, 4.9 8, 19.7	1 ℓ	$\ell + \tau_h \tau_h$	-0.33 ± 1.02	x	BDT based on $p_T^{\text{had,lead}}$ Split $p_T^{\ell_1} + p_T^{\ell_2} + p_T^\tau$ at 130 GeV
	2 ℓ			$e^\pm \mu^\pm + \tau_h$	x			
	[26]	CMS	13, 35.9	1 ℓ	$\ell + \tau_h \tau_h$	$3.39^{+1.68}_{-1.54}$	✓(Wh)	
	2 ℓ			$e^\pm \mu^\pm + \tau_h$				
	$\gamma\gamma$	[27]	ATLAS	7, 5.4 8, 20.3	$\ell\nu$ $\cancel{\nu}, \nu\nu$ jj	One-lepton E_T^{miss} Hadronic	1.0 ± 1.6	x
[28]		CMS	7, 5.1 8, 19.7	$\ell\nu$ $\cancel{\nu}, \nu\nu$ jj	One-lepton E_T^{miss} Hadronic	$-0.16^{+1.16}_{-0.79}$	x	Split E_T^{miss} at 45 GeV $E_T^{\text{miss}} > 70$ GeV $p_T^{\gamma\gamma} > 13m_{\gamma\gamma}/12$
[29]				ATLAS	13, 139			
[30]		CMS	13, 35.6	$\ell\nu$ $\cancel{\nu}, \nu\nu$ jj	One-lepton E_T^{miss} Hadronic	$3.0^{+1.5}_{-1.3}$ - $5.1^{+2.5}_{-2.3}$	x x ✓(Vh)	Superseeded by full Run 2 result $E_T^{\text{miss}} > 85$ GeV $p_T^{\gamma\gamma}/m_{\gamma\gamma}$ not used
[31]				CMS	13, 137	$\ell\nu$ jj	One-lepton Hadronic	$1.31^{+1.42}_{-1.12}$ $0.89^{+0.89}_{-0.91}$
[32]		ATLAS	13, 139			$\ell\ell\ell\ell + \ell\nu$ $\ell\ell\ell\ell + q\bar{q}$	Lep-enriched 2j	$1.44^{+1.17}_{-0.93}$
[33]		CMS	13, 137.1	$\ell\ell\ell\ell + \ell\nu$	Lep-low p_T^h	$3.21^{+2.49}_{-1.85}$	✓(Vh)	$p_T^h < 150$ GeV
$\ell\ell\ell\ell + q\bar{q}$				Lep-high p_T^h	$0.00^{+1.57}_{-0.00}$	x	$p_T^h > 150$ GeV	
					2j	$0.57^{+1.20}_{-0.57}$	x	$60 < m_{jj} < 120$ GeV

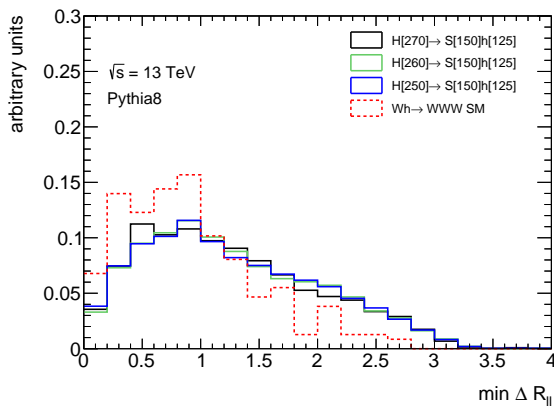
Table 1 Summary of ATLAS and CMS Vh results. The “-” symbol indicates that the signal strength result is not provided for that specific category.

is used. An important BDT input discriminating variable is the invariant mass of the lepton with different electric charge and the lepton originated from the W boson radiating the SM Higgs particle ($m_{\ell_0\ell_2}$). This quantity tends to lower values for $H \rightarrow Sh$ events compared with the Wh process as shown in Figure 1a for events with exactly three

leptons with $p_T > 25, 20, 15$ GeV and total electric charge of ± 1 . The same behavior is also observed for WZ^* and Z +jets events. These are the dominant background contributions for this category and they are mostly located in the $m_{\ell_0\ell_2} < 100$ GeV region. Given this feature, it is expected that the BDT discriminates these SM background processes,



(a)



(b)

Fig. 1 Invariant mass of the lepton with different electric charge and the lepton originating from the W boson radiating the SM Higgs particle (a) and minimal distance between leptons (b) in the Wh 3ℓ channel for several $H \rightarrow Sh$ samples (solid lines) compared with the SM Vh process with $h \rightarrow WW$ (dashed line) generated with PYTHIA8. The last bin contains overflow events.

as well as the $H \rightarrow Sh$ signal, to the benefit of the target decay: $Wh \rightarrow WWW$. In light of this, the observed signal strength in 1SFOS events will not be combined with results from other categories.

ATLAS has also published more recent Wh results using 36.1 fb^{-1} from the Run 2 dataset [21] for which only 3ℓ channels are considered. The selection strategy follows that from Run 1, but the usage of multivariate techniques has also been extended to the 0SFOS channel. In this case two BDTs are developed to reject WZ and $t\bar{t}$ events. Mostly leptonic kinematic variables are used as inputs to the BDT against WZ backgrounds in the 0SFOS category from which only three are common to the 1SFOS category: the invariant mass of the Higgs lepton candidates, E_T^{miss} and the difference in pseudo-rapidity between the leptons with the same electric charge. The BDT against $t\bar{t}$ uses as input variables hadronic quantities such as the number of jets and the transverse momentum of the jet with highest p_T . The observed

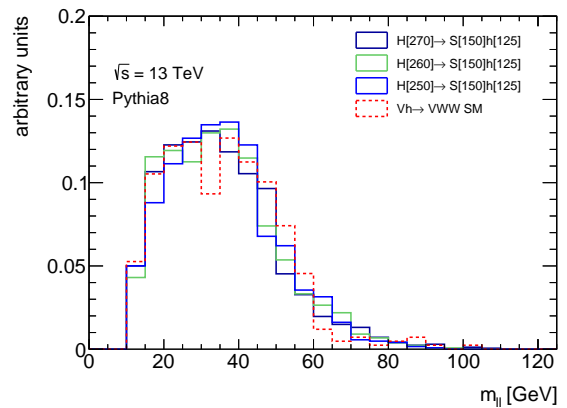


Fig. 2 Di-lepton invariant mass for several $H \rightarrow Sh$ samples (solid lines) compared with the SM Vh process with $h \rightarrow WW$ (dashed line) generated with PYTHIA8.

signal strength combining all 3ℓ channels shows a deviation of about 2σ with respect to the SM expectation, as quoted in Table 1, and it will be used in the combination in Section 5. Although the channel with at least 1SFOS lepton pair still makes use of the $m_{\ell_0 \ell_2}$ as the BDT input discriminating variable, it can not be isolated and excluded from the Vh combination exercise. It is important to note that the 0SFOS category alone would provide a higher discrepancy, as in this case the $H \rightarrow Sh$ is not expected to be rejected by the selection criteria. However, the observed signal strength result from Ref. [21] combines both categories so the result for 0SFOS events can not be accounted for separately.

The CMS collaboration has also published results for the Vh production mode with $h \rightarrow WW^*$ decay using Run 1 and partial Run 2 datasets [22, 23]. In these results a Vh tagged category is defined by selecting events with a DFOS lepton pair with at least two jets in the final state. Similar to the ATLAS Run 1 strategy, m_{jj} is used to guarantee the consistency with the parent boson mass and $|\Delta\eta_{jj}| < 3.5$ is applied to avoid overlap with VBF events. In addition, the leptons are required to have small $\Delta R_{\ell\ell}$ since they are expected to be emitted in nearby directions due to the spin-0 nature of the SM Higgs boson. Finally, m_T is required to be between 60 GeV and the mass of the SM Higgs boson. The $m_{\ell\ell}$ distribution is used as an input for the template fit to obtain the signal strength results. Both Run 1 and Run 2 results show a discrepancy between the observed data and the SM expectation at $m_{\ell\ell} < 50$ GeV. The SM Higgs boson as well as the $H \rightarrow Sh$ process are both expected to concentrate at the low $m_{\ell\ell}$ region as shown in Figure 2. As quoted in Table 1, the signal strength is below unity for the Run 1 analysis, while the observed Run 2 data presents an excess of $\sim 2.2\sigma$. Since the selection is the same in both cases there is no reason to select one result and reject the other. In light of the CMS event selection, the observed signal strengths

from the DFOS category using Run 1 and Run 2 datasets will both be used in the combination.

Finally, CMS also targets events in the 3ℓ category which are further split into two subcategories based on the existence of SFOS lepton pairs in the triplet. Opposite to ATLAS, the use of multivariate techniques is not considered by the CMS strategy. To reduce Drell-Yan processes a lower bound on the E_T^{miss} and a Z boson veto are applied for 1SFOS events. The observed signal strength for this category is extracted using the minimum $\Delta R_{\ell\ell}$ between oppositely charged leptons in the likelihood fit (see Figure 1b). Table 1 shows the same trend as previously discussed for the 2ℓ channel: Run 1 results present a signal strength below one but fully consistent with the SM due to the large uncertainty. The situation is the opposite with the partial Run 2 dataset for which the signal strength is above unity, with a deviation from the SM expectation of $\sim 1.3\sigma$. As discussed for the 2ℓ category, both Run 1 and Run 2 results from CMS will be included in the combination.

3.2 $Wh \rightarrow W\tau\tau$

Results for the associated production of the SM Higgs boson with a W boson, where the Higgs boson is decaying into a pair of tau leptons have been performed by the ATLAS and CMS collaborations. The strategy in both experiments split the events into two categories, depending on the number of tau leptons decaying to hadrons (τ_{had}), while the W boson is assumed to decay leptonically. In the first category, the selection requires one electron and one muon with the same electric charge; and the presence of one τ_{had} candidate in the final state ($e^\pm\mu^\pm\tau_{\text{had}}$). The second category selects events having one electron or muon accompanied by two τ_{had} candidates from the SM Higgs decay ($\ell\tau_{\text{had}}\tau_{\text{had}}$).

The results from ATLAS are obtained using the Run 1 dataset [24]. The kinematic selection for the $e^\pm\mu^\pm\tau_{\text{had}}$ category requires the scalar sum of the p_T of the electron, muon and τ_{had} to be greater than 80 GeV. Figure 3a shows the scalar sum of the leptons' p_T for events with exactly one electron and one muon satisfying $p_T^\ell > 20, 10$ GeV; and one hadronic tau with $p_T^\tau > 20$ GeV. It is clear that the lower bound threshold on this quantity keeps most of the Wh and $H \rightarrow Sh$ processes. In the $\ell\tau_{\text{had}}\tau_{\text{had}}$ category the transverse mass of the lepton and E_T^{miss} is required to be above 20 GeV and the two τ_{had} candidates must be within a ΔR of 2.8. Finally, the scalar sum of the p_T of the lepton and the two τ_{had} is required to be above 100 GeV. Figure 3b compares the spectrum of this variable for events with one electron or muon with $p_T^\ell > 24$ GeV and two hadronic taus satisfying $p_T^\tau > 25, 20$ GeV. Based on the kinematic selection used in these ATLAS Run 1 results, it is expected similar selection efficiency for both Wh and $H \rightarrow Sh$ processes, so these results will be used in the combination. The observed signal

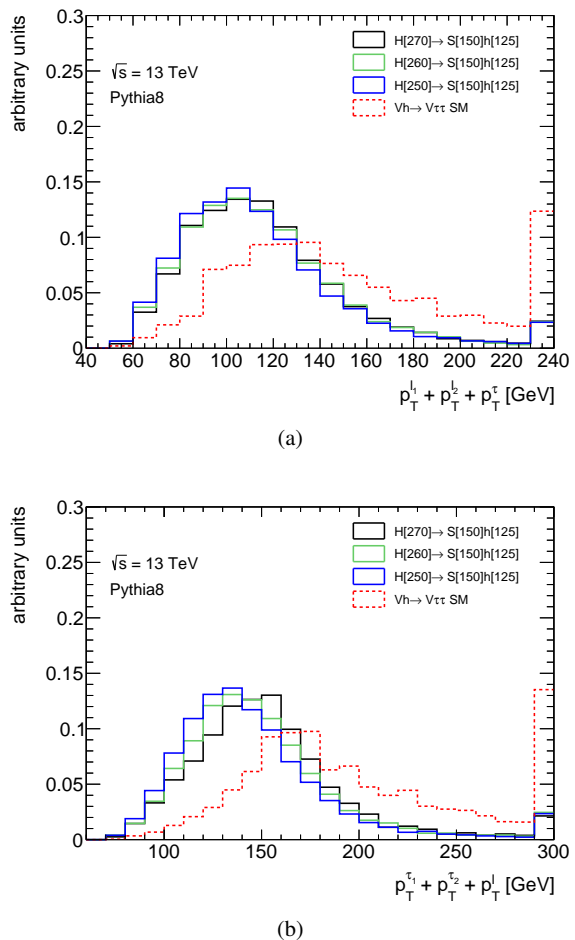


Fig. 3 Scalar sum of the transverse momentum of two leptons and a hadronic tau (a) and scalar sum of the of transverse momentum of the lepton and two hadronic taus (b) for several $H \rightarrow Sh$ samples (solid lines) compared with the SM Vh process with $h \rightarrow \tau\tau$ (dashed line) generated with PYTHIA8. The last bin contains overflow events.

strength in each category is determined from a fit to the reconstructed Higgs boson candidate mass distribution, resulting in values above unity with relatively large uncertainties, as shown in Table 1.

Results for the associated production with a W boson of the SM Higgs particle, when it decays to a pair of tau leptons, has been delivered by the CMS experiment using Run 1 and Run 2 data [25, 26]. However, the strategy and event selection is different for each dataset, and in the following they will be described. On the one hand, the $\ell\tau_{\text{had}}\tau_{\text{had}}$ category in CMS Run 1 results makes use of a BDT discriminant based on the E_T^{miss} and on kinematics related to the di-tau system. In addition, the input discriminating variables include the transverse momentum of the two hadronic taus. Figure 4 compares the shapes of the transverse momentum of the leading hadronic tau for both Wh and $H \rightarrow Sh$ processes. Given the fact that the $H \rightarrow Sh$ signal tends to be located at the low p_T region where the reducible processes

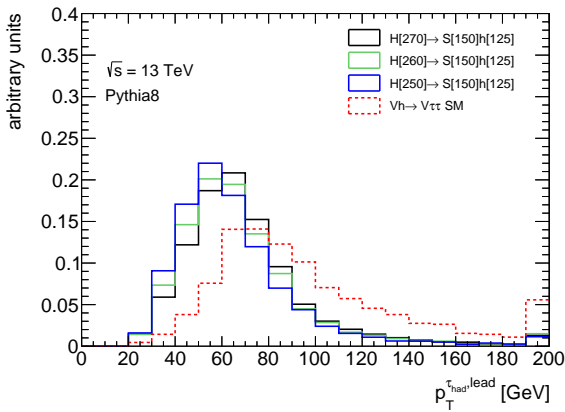


Fig. 4 Transverse momentum of the leading hadronic tau for several $H \rightarrow Sh$ samples (solid lines) compared with the SM Vh process with $h \rightarrow \tau\tau$ (dashed line) generated with PYTHIA8. The last bin contains overflow events.

such as QCD multilepton, $W/Z+\text{jets}$, $W/Z+\gamma$, and $t\bar{t}$ mostly contribute, it is expected that the BDT discriminates these backgrounds together with the $H \rightarrow Sh$ signal in benefit of the SM Wh process. On the other hand, the $e^\pm\mu^\pm\tau_{\text{had}}$ category is further split into two by dividing the scalar sum of the leptons' p_T at 130 GeV. The likelihood fit is performed using the invisible mass of the Higgs decay lepton candidates in each $p_T^e + p_T^\mu + p_T^\tau$ region. Figure 3a shows that the contribution for the BSM process concentrates at the low region and the Wh signal is distributed uniformly in these two regions. Due to the fact that the SM backgrounds are dominant in the low region, the statistical fit procedure tends to extract the Wh signal strength from the high region where the Wh signal over background ratio is higher. Since this region has higher impact in the statistical fit it clearly drives the $\mu(Wh)$ result. The BSM hypothesis concentrates at the low region so it is expected that it does not contribute significantly to these results. In light of these features, the Run 1 results from CMS for the Wh with $h \rightarrow \tau\tau$ are not considered for the signal strength combination in this paper.

The CMS strategy for the analysis of the Run 2 dataset follows a different approach. The category with one τ_{had} in the final state requires the scalar sum of the p_T of the leptons and the τ_{had} to be above 100 GeV. From Figure 3a it can be seen that the $H \rightarrow Sh$ efficiency after this cut is applied is above 70%. The Higgs and W bosons are expected to be close in η , since they are dominantly produced back-to-back in ϕ and they may have a longitudinal Lorentz boost. As such, two angular separation cuts between the highest p_T lepton and the system formed by the τ_{had} and the remaining lepton are applied. In the $\ell\tau_{\text{had}}\tau_{\text{had}}$ category, the threshold on the scalar sum of the lepton and the two τ_{had} is 130 GeV. As shown in Figure 3b, this cut still keeps about 60% of the $H \rightarrow Sh$ process. In addition, the vectorial sum of p_T of the lepton, the two τ_{had} candidates and the E_T^{miss} is required

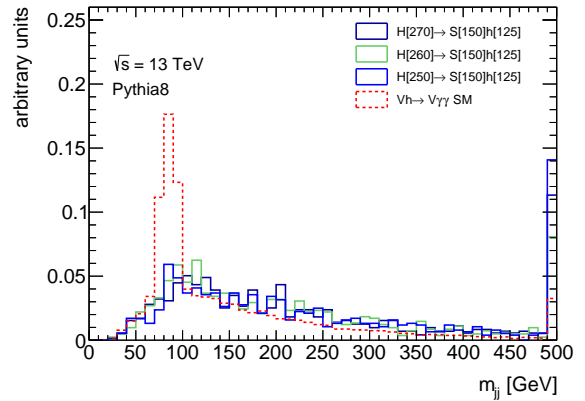


Fig. 5 Dijet invariant mass in events with two photons and at least two jets for several $H \rightarrow Sh$ samples (solid lines) compared with the SM Vh process with $h \rightarrow \gamma\gamma$ (dashed line) generated with PYTHIA8. The last bin contains overflow events.

to be below 70 GeV. Finally, only events with small angular separation of the two τ_{had} candidates in η are selected. Given the fact that the event selection is not expected to affect the $H \rightarrow Sh$ efficiency dramatically, this result should be used in the combination. The observed signal strength for this case presents a deviation with respect to the SM expectation of about 1.4σ , as shown in Table 1.

3.3 $Wh \rightarrow W\gamma\gamma$

Results for the associated production of a W/Z boson with the SM Higgs particle when the latter decays into a pair of photons have also been released by the ATLAS and CMS collaborations using both Run 1 and Run 2 datasets [27–31]. The selection criteria in both cases exploit the different vector boson decays by requiring the presence of leptons, jets or E_T^{miss} in the final state. The events are classified into three main categories: Wh one-lepton, Vh hadronic and $Vh E_T^{\text{miss}}$.

Events in the Vh hadronic category are required to have a pair of high-energy jets originating from the vector boson decay, hence with m_{jj} consistent with the V boson mass. Figure 5 compares the invariant mass of the dijet system for the SM Higgs boson associated production and the $H \rightarrow Sh$ process. The selected events contain two photons with $p_T^{\gamma_0} > m_{\gamma\gamma}/2$ and $p_T^{\gamma_1} > m_{\gamma\gamma}/4$, and at least two jets with transverse momentum above 40 GeV. For the Vh process the efficiency reaches more than 50% when selecting an m_{jj} window cut in the range of [60 – 120] GeV. For the BSM process of interest here, the m_{jj} selection keeps around 20% of the total statistics.

ATLAS Run 1 analysis uses the magnitude of the component of the diphoton momentum transverse to its thrust axis in the transverse plane ($p_T^{\gamma\gamma}$). The strategy selects events with m_{jj} in the [60 – 110] GeV range and $p_T^{\gamma\gamma}$ above 70 GeV.

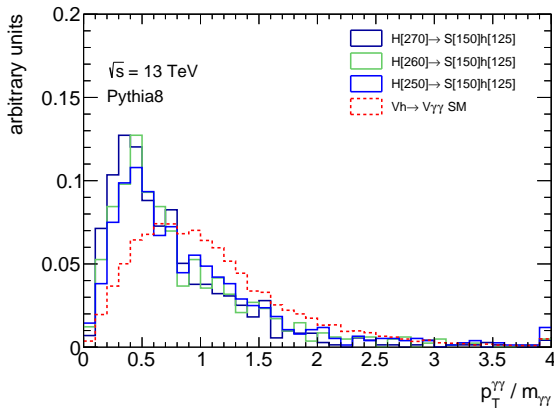


Fig. 6 Ratio between the transverse momentum and the invariant mass of the diphoton system in events with at least two jets for several $H \rightarrow Sh$ samples (solid lines) compared with the SM Vh process with $h \rightarrow \gamma\gamma$ (dashed line) generated with PYTHIA8. The last bin contains overflow events.

The ATLAS Run 1 results for the Vh hadronic category are not included in the combination due to the high $p_T^{\gamma\gamma}$ threshold in addition to the restricted m_{jj} window requirement. In Run 2 the ATLAS measurements are carried out using 139 fb^{-1} of pp collision data at $\sqrt{s} = 13 \text{ TeV}$ and the Higgs boson production mechanisms are further characterised in terms of the Simplified Template Cross-Section (STXS) framework [36–39]. In this case two m_{jj} regions inclusive in the transverse momentum of the SM Higgs boson are considered. In the first region to tag the hadronic decay of the vector boson the m_{jj} is required to be between $[60 - 120] \text{ GeV}$, similarly to the Run 1 strategy. This result will not be considered in the combination due to the low acceptance of the BSM process in this m_{jj} range, as shown in Figure 5. A second STXS region considers events outside the m_{jj} window: $m_{jj} \in [0, 60] \cup [120, 350] \text{ GeV}$ where the majority of the $H \rightarrow Sh$ events are expected to contribute. In this case the observed signal strength is $3.16^{+1.84}_{-1.72}$ and this result will be included in the final combination.

Results from CMS make use of the angle between the diphoton and the diphoton-dijet system in both Run 1 and Run 2 datasets. The main difference between the CMS strategies is the use of the $p_T^{\gamma\gamma}/m_{\gamma\gamma}$ quantity. In CMS Run 1 [28] analysis, events are required to satisfy $p_T^{\gamma\gamma} > 13m_{\gamma\gamma}/12$ for the Vh hadronic category. Figure 6 shows the ratio between the diphoton transverse momentum and its invariant mass. The $p_T^{\gamma\gamma}/m_{\gamma\gamma}$ requirement highly reduces the $H \rightarrow Sh$ acceptance by rejecting more than 85% of the BSM events. Similarly, the full Run 2 strategy [31] considers the $p_T^{\gamma\gamma}/m_{\gamma\gamma}$ quantity as input variable in the BDT. Due to the SM Vh spectrum in Figure 6 it is expected that the BDT discriminates the low $p_T^{\gamma\gamma}/m_{\gamma\gamma}$ region where the background and the $H \rightarrow Sh$ processes dominate. In light of this, the CMS Run 1 as well as the full Run 2 results will not be considered

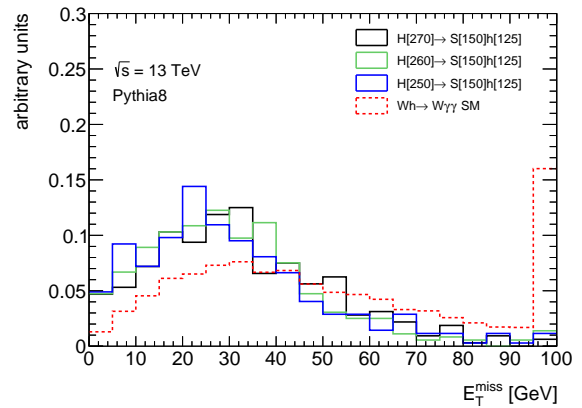
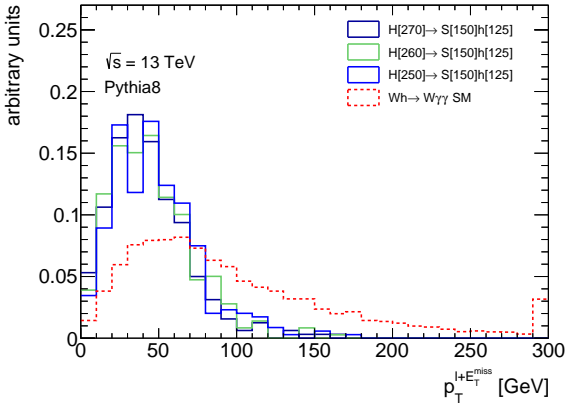


Fig. 7 Missing transverse energy in events with two photons and one electron or muon for several $H \rightarrow Sh$ samples (solid lines) compared with the SM Wh process with $h \rightarrow \gamma\gamma$ (dashed line) generated with PYTHIA8. The last bin contains overflow events.

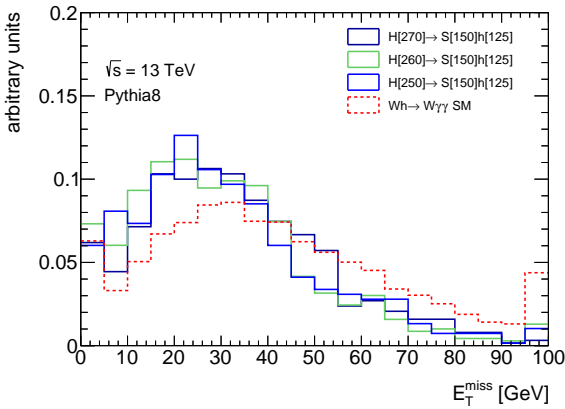
in the combination. However, the $p_T^{\gamma\gamma}/m_{\gamma\gamma}$ requirement was dropped in the partial Run 2 results using 35.9 fb^{-1} [30]. The measurement for the Vh hadronic category in this case presents a deviation from the SM expectation of approximately 1.5σ , being the observed signal strength $5.1^{+2.5}_{-2.3}$. This result will be included in the final combination.

The Vh E_T^{miss} category is enriched in events with a leptonic decay of the W boson, when the lepton is not detected or does not satisfy the selection criteria (denoted by $\cancel{\ell}$), or with a Z boson decaying into a pair of neutrinos. In this case the selection criteria relies on the E_T^{miss} distribution to select events in the high range. The strategy from CMS uses a lower bound of $85(70) \text{ GeV}$ on the E_T^{miss} for Run 2(1) results. Similarly, ATLAS Run 1 results are obtained by applying a cut on a E_T^{miss} based quantity which is approximately equivalent to a $E_T^{\text{miss}} > 70 - 100 \text{ GeV}$ requirement.

The Wh one-lepton class is characterised by a leptonically decaying W boson, hence it targets events with two photons accompanied by one electron or one muon. CMS further splits the one-lepton category by dividing the E_T^{miss} spectrum at 45 GeV [28]. Figure 7 shows the missing transverse energy for events with two photons and a lepton. At this cut value, the Wh process is divided by 50% in each region, with the events in the high E_T^{miss} range the ones driving the result on the measured signal strength. The $H \rightarrow Sh$ signal acceptance is approximately 20% in the high E_T^{miss} region. The CMS Run 1 results will be discarded in the combination as they are computed including not only the Vh one-lepton category but also the hadronic and E_T^{miss} ones as well. Conversely, CMS full Run 2 results are produced in the Higgs STXS framework and delivered for the one-lepton and the hadronic categories separately. In addition, two regions are defined using the transverse momentum of the V boson ($p_T^{l+E_T^{\text{miss}}}$) at 75 GeV for the leptonic category. Only the $p_T^{l+E_T^{\text{miss}}} < 75 \text{ GeV}$ result will be considered as the mea-



(a)



(b)

Fig. 8 Transverse momentum of the lepton and the E_T^{miss} system in events with two photons and a lepton (a) and missing transverse energy after requiring $p_T^{\ell+E_T^{\text{miss}}} < 150$ GeV (b) for several $H \rightarrow Sh$ samples (solid lines) compared with the SM Wh process with $h \rightarrow \gamma\gamma$ (dashed line) generated with PYTHIA8. The last bin contains overflow events.

sured signal strengths are provided for each analysis category and the contribution of the BSM process is dominant in the low region, as shown in Figure 8a. The Run 2 CMS result measures an observed signal strength for the Wh one-lepton category of $1.31^{+1.42}_{-1.12}$ [31].

The full Run 2 ATLAS strategy for the Wh leptonic category builds a BDT with photon and lepton variables used as input [29]. In addition, E_T^{miss} related quantities and vector-boson kinematics are also used as input variables in the BDT. The Wh one-lepton events are split using the transverse momentum of the lepton and the E_T^{miss} at 150 GeV. Figure 8a compares the shape of the $p_T^{l+E_T^{\text{miss}}}$ quantity for Wh and $H \rightarrow Sh$ processes. The contribution of the BSM signal in the high region of the distribution is expected to be negligible so this result will not be considered in the combination. However the $H \rightarrow Sh$ process is almost entirely located at $p_T^{l+E_T^{\text{miss}}} < 150$ GeV. Since the E_T^{miss} is used in the BDT it

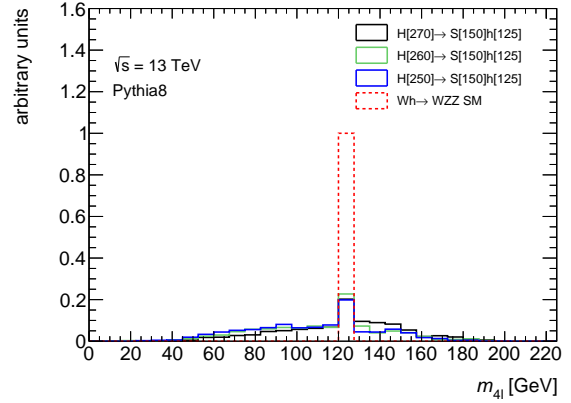


Fig. 9 Invariant mass of the four leptons for several $H \rightarrow Sh$ samples (solid lines) compared with the SM Wh process with $h \rightarrow ZZ \rightarrow 4\ell$ (dashed line) generated with PYTHIA8. The last bin contains overflow events.

is important to verify that in the low $p_T^{l+E_T^{\text{miss}}}$ region the performance of the distribution is similar for the $H \rightarrow Sh$ and SM Wh processes. Figure 8b shows the E_T^{miss} distribution in events with two photons and one electron or muon after requiring $p_T^{\ell+E_T^{\text{miss}}} < 150$ GeV. It can be observed that the spectrum for each process is similar being the mean of the distributions 39 GeV and 31 GeV for the SM Wh and $H \rightarrow Sh$ signals, respectively. The full Run 2 ATLAS result in the low $p_T^{l+E_T^{\text{miss}}}$ phase space presents a deviation from the SM value of $\sim 2\sigma$. The observed signal strength is $2.41^{+0.71}_{-0.70}$ and this measurement will be included in the combination. The ATLAS strategy for the Run 1 dataset selects Wh one-lepton events by applying a cut on a E_T^{miss} related quantity. In light of this requirement and the difference between the SM and BSM processes as shown in Figure 7, the ATLAS Run 1 results for the one-lepton category are not included in the final combination.

3.4 $Wh \rightarrow WZZ$

ATLAS and CMS results for the $H \rightarrow ZZ^* \rightarrow 4\ell$ decay mode using the full Run 2 dataset are published in Ref. [32] and Ref. [33], respectively. The common strategy makes use of the invariant mass of the four leptons from the Higgs decay ($m_{4\ell}$) to select the Higgs candidates in a window around its mass: $115 \text{ GeV} < m_{4\ell} < 130 \text{ GeV}$. Approximately 70% of the $H \rightarrow Sh$ events are outside this $m_{4\ell}$ mass window so this requirement highly reduces the acceptance of the BSM signal as shown in Figure 9. Both experiments split the events depending on the hadronic or leptonic decay of the V boson produced in association with the Higgs boson. In the hadronic channel, the four leptons from the Higgs decay are accompanied by two jets and the m_{jj} distribution is exploited. CMS selects events in the window around the W/Z

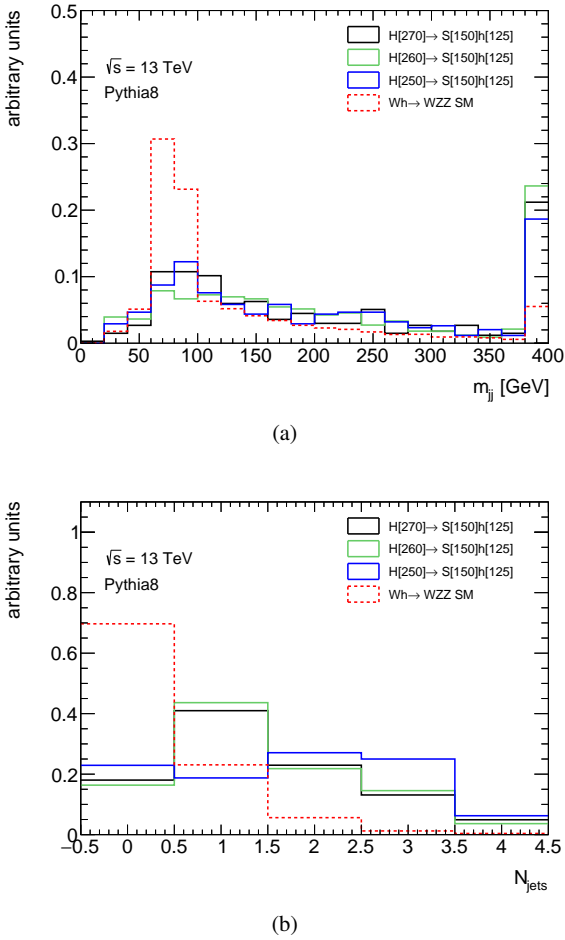


Fig. 10 Dijet invariant mass (a) and jet multiplicity (b) for several $H \rightarrow Sh$ samples (solid lines) compared with the SM Wh process with $h \rightarrow ZZ \rightarrow 4\ell$ and $W \rightarrow q\bar{q}$ (dashed line) generated with PYTHIA8. The last bin contains overflow events.

mass peak: $60 \text{ GeV} < m_{jj} < 120 \text{ GeV}$ and ATLAS uses the m_{jj} spectrum as input in a neural network (NN) to separate between the Vh and VBF production mechanisms. Given the dependence of the SM results on the m_{jj} spectrum it is expected that these measurements do not include the $H \rightarrow Sh$ signal. Figure 10a compares the m_{jj} distribution for the SM Wh and the $H \rightarrow Sh$ processes for events with four leptons and two jets in the final state. The rejection of the BSM process is approximately 70% when requiring events within the range $60 \text{ GeV} < m_{jj} < 120 \text{ GeV}$. Since ATLAS and CMS strategies rely on the m_{jj} window the results for the hadronic category will not be included in the combination.

In the Wh leptonic category, the analyses require an extra lepton in the final state. ATLAS strategy uses variables as the jet and b -tagged jet multiplicities, in addition to the E_T^{miss} distribution, to build a MVA discriminant to distinguish between Vh and tth production mechanisms. Figure 10b compares the distributions of the expected number of jets with $p_T > 30 \text{ GeV}$ for the SM and the BSM processes from MC

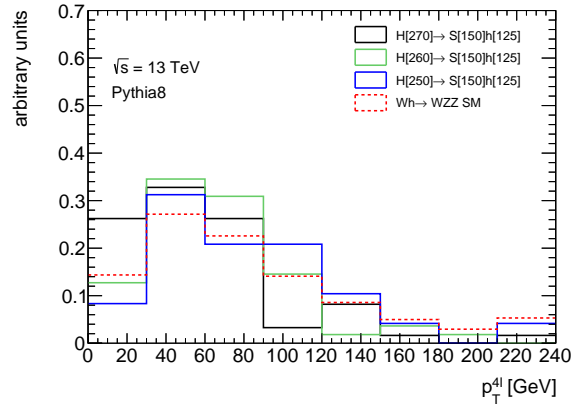


Fig. 11 Transverse momentum of the leptons associated to the SM Higgs decay for the $H \rightarrow Sh$ samples (solid lines) compared with the SM Wh process with $h \rightarrow ZZ \rightarrow 4\ell$ and $W \rightarrow \ell\nu$ (dashed line) generated with PYTHIA8. The last bin contains overflow events.

simulation. Events from the Wh decay are dominant at low jet multiplicities, being the contribution of events with zero jets of around 70%. Conversely, the $H \rightarrow Sh$ signal tends to have higher number of jets and it only contributes $\sim 20\%$ in events with no jets in the final state. Due to the expected differences in the jet multiplicity distribution between the SM and BSM processes the ATLAS results for the leptonic category are not combined with the rest of Wh results.

Finally, for the leptonic category CMS selects events with at most three jets, hence it is expected a high acceptance of the $H \rightarrow Sh$ signal which can be seen from Figure 10b. In addition, the final candidate events are split into two regions of the Higgs transverse momentum: $p_T^{4\ell} < 150 \text{ GeV}$ and $p_T^{4\ell} > 150 \text{ GeV}$. Figure 11 shows the transverse momentum of the four leptons associated to the SM Higgs decay. For both SM Wh and $H \rightarrow Sh$ processes the bulk of the events is located in the low $p_T^{4\ell}$ region. In light of the $p_T^{4\ell}$ distribution, only the measured signal strength for the $p_T^{4\ell} < 150 \text{ GeV}$ region will be included in the final combination. The observed cross section in this case normalised to the SM prediction results in $3.21^{+2.49}_{-1.85}$ from Ref. [33].

4 Compatibility with inclusive observables

While this paper focuses on the anomalous production of the SM Higgs boson in association with leptons, it is relevant to investigate if these findings do not contradict measurement of inclusive observables made by the experiments. It is known that the additional production of the SM Higgs boson via the $H \rightarrow Sh$ process would distort the h transverse momentum and the rapidity spectra. The transverse momentum would be enhanced at moderate values. The SM Higgs boson would be produced more centrally. A survey of available Run 1 and Run 2 data was performed [40–46]. All data sets, except the ATLAS Run 2 $h \rightarrow ZZ^* \rightarrow 4\ell$ results, dis-

play compatibility with these features concurrently. While the overall deviation from the SM hypothesis is not statistically significant (of order of two standard deviations), it is compatible with the hypothesis considered here. A comprehensive analysis of inclusive observables will be performed when the complete Run 2 data set is available.

5 Results and Conclusions

The interpretation of the multi-lepton anomalies at the LHC reported in Refs. [1, 2] with the decay $H \rightarrow Sh$ predicts anomalously large values of the signal strength of Wh . This effect should be visible with the available results from ATLAS and CMS so far. Section 3 provides a comprehensive synopsis of the current status of the search and measurements of Wh production in the SM, where the available results correspond to the Run 1 and, partial or complete, Run 2 data sets. Table 1 gives the summary of the available results and indicates which ones are used in the combination with the appropriate explanation. The combination is estimated as the error weighted signal strength of each considered result. The uncertainties between different channels, for both experiments and across data sets are treated as uncorrelated. The obtained result is then compared with the one expected for the SM scenario with $\mu = 1$. By using the method given in Particle Data Group to combine different measurements with asymmetric uncertainties [47] the combined Wh signal strength from Table 1 results in $\mu(Wh)_{Inc} = 2.41 \pm 0.37$ which corresponds to a deviation from the SM of 3.8σ .¹ The errors are dominated by statistical and experimental uncertainties, which are uncorrelated. The bulk of the correlated uncertainties pertain to the theoretical error, which for this production mechanism is significantly smaller than the error claimed here.

As discussed in Section 3, the estimate made here is based on searches and measurements biased towards the SM. The combination of the rejected measurements from Table 1 results in $\mu(Wh)_{Rej} = 0.95 \pm 0.35$. In the corners of the phase-space where the BSM signal is not expected to contribute, the signal strength of the Wh production is consistent with the SM prediction. Combining all the results provides a signal strength of $\mu(Wh)_{All} = 1.64 \pm 0.25$, which corresponds to a deviation from the SM value of unity of 2.6σ .

The impact on the measurement of h cross-sections due to the BSM signal considered here goes beyond the associated production of leptons, as discussed here. The measurement of the Higgs boson transverse momentum and rapidity will also be affected. These effects will be studied with results with the full Run 2 data set, when available.

¹Also by removing the channels that are based on BDTs, such as in Ref. [21] and the one-lepton category in Ref. [29], the combined result is $\mu(Wh)_{No-BDT} = 2.39 \pm 0.44$ which corresponds to a deviation of 3.2σ from the SM.

While the effect seen here seems in qualitative agreement with the multi-lepton anomalies interpreted with the simplified model described in Section 2, it is important to confront the value of $\mu(Wh)_{Inc}$ with that expected with the ansatz of $\text{Br}(H \rightarrow Sh) = 100\%$ made in Refs. [1, 2]. Assuming the cross-section $\sigma(H \rightarrow S^*h) = 10 \text{ pb}$ [12], where h is on-shell, one would expect a combined (including the SM) signal strength of about 6 for the combination of the channels considered in Section 3. This is considerably larger than the signal strength observed here, notwithstanding the expected bias discussed in Section 3. This indicates that explaining the multi-lepton anomalies reported in Refs. [1, 2] would require a considerable contribution from $H \rightarrow SS$ along with $H \rightarrow Sh$. The decay $H \rightarrow hh$ would be suppressed due to results from direct searches.

Irrespective of the size of $\mu(Wh)_{Inc}$ determined here, one needs to seriously consider a situation whereby the production of h at the LHC is contaminated with production mechanisms other than those predicted in the SM. This implies that the determination of couplings of h to SM particles would be seriously compromised by model dependencies. This further enhances the physics case of Higgs factories on the basis of e^+e^- [48–50] and e^-p [51–54] collisions, while the potential for the direct observation of new physics at the HL-LHC is enriched strongly. The production of H in e^-p collisions would be suppressed, therefore, the determination of the Higgs boson couplings would be less model dependent compared to proton-proton collisions. Assuming the current value of the h global signal strength at the LHC, and that the couplings of h to SM particles are as in the SM, the contamination at the LHeC would be five times smaller than that at the LHC [55]. The LHeC, with input from proton-proton collisions, would allow for the precise determination of the hWW coupling, which combined with the superb measurement of the hZZ coupling in e^+e^- collisions, would provide a powerful probe into EWSB.

6 Acknowledgements

The authors are grateful for support from the South African Department of Science and Innovation through the SA-CERN program and the National Research Foundation for various forms of support. The authors are also indebted to the Research Office of the University of the Witwatersrand for grant support. This work was supported by the Beijing Municipal Science and Technology Commission project (Grant No.: Z191100007219010).

References

1. S. von Buddenbrock, A. S. Cornell, A. Fadol, M. Kumar, B. Mellado and X. Ruan, J. Phys. G **45**, no. 11, 115003

- (2018) [arXiv:1711.07874 [hep-ph]].
2. S. Buddenbrock, A. S. Cornell, Y. Fang, A. Fadol Mohammed, M. Kumar, B. Mellado and K. G. Tomiwa, *JHEP* **1910**, 157 (2019) [arXiv:1901.05300 [hep-ph]].
 3. S. von Buddenbrock, N. Chakrabarty, A. S. Cornell, D. Kar, M. Kumar, T. Mandal, B. Mellado, B. Mukhopadhyaya, R. G. Reed and X. Ruan, *Eur. Phys. J. C* **76**, no.10, 580 (2016) [arXiv:1606.01674 [hep-ph]].
 4. P. W. Higgs, *Phys. Lett.* **12**, 132 (1964).
 5. F. Englert and R. Brout, *Phys. Rev. Lett.* **13**, 321 (1964).
 6. P. W. Higgs, *Phys. Rev. Lett.* **13**, 508 (1964).
 7. G. S. Guralnik, C. R. Hagen and T. W. B. Kibble, *Phys. Rev. Lett.* **13**, 585 (1964).
 8. ATLAS Collaboration, *Phys. Lett. B* **716**, 1 (2012) [arXiv:1207.7214 [hep-ex]].
 9. CMS Collaboration, *Phys. Lett. B* **716**, 30 (2012) [arXiv:1207.7235 [hep-ex]].
 10. CMS Collaboration, *Phys. Rev. Lett.* **110**, no. 8, 081803 (2013) [arXiv:1212.6639 [hep-ex]].
 11. ATLAS Collaboration, *Phys. Lett. B* **726**, 120 (2013) [arXiv:1307.1432 [hep-ex]].
 12. Y. Fang, M. Kumar, B. Mellado, Y. Zhang and M. Zhu, *Int. J. Mod. Phys. A* **32**, no. 34, 1746010 (2017) [arXiv:1706.06659 [hep-ph]].
 13. S. von Buddenbrock, A. S. Cornell, E. D. R. Iarilala, M. Kumar, B. Mellado, X. Ruan and E. M. Shrif, *J. Phys. G* **46**, no. 11, 115001 (2019) [arXiv:1809.06344 [hep-ph]].
 14. M. Muhlleitner, M. O. P. Sampaio, R. Santos and J. Wittbrodt, *JHEP* **1703**, 094 (2017) doi:10.1007/JHEP03(2017)094 [arXiv:1612.01309 [hep-ph]].
 15. CMS Collaboration, *Phys. Rev. Lett.* **121**, 121801 (2018) [arXiv:1808.08242 [hep-ex]].
 16. ATLAS Collaboration, *Phys. Lett. B* **786** 59 (2018) [arXiv:1808.08238 [hep-ex]].
 17. T. Sjöstrand, S. Mrenna, and P. Z. Skands, *Comput. Phys. Commun.* **178** 852-867 (2008) [arXiv:0710.3820 [hep-ph]].
 18. Ball, Richard D. *et al.*, *Nucl. Phys. B* **867** (2013) [arXiv:1207.1303 [hep-ph]].
 19. ATLAS Collaboration, ATL-PHYS-PUB-2014-021 (2014) [https://cds.cern.ch/record/1966419].
 20. ATLAS Collaboration, *JHEP* **08** (2015) 137, [arXiv:1506.06641 [hep-ex]].
 21. ATLAS Collaboration, *Phys. Lett. B* **798** (2019) 134949, [arXiv:1903.10052 [hep-ex]].
 22. CMS Collaboration, *JHEP* **01** (2014) 096, [arXiv:1312.1129 [hep-ex]].
 23. CMS Collaboration, *Phys. Lett. B* **791** (2019) 96, [arXiv:1806.05246 [hep-ex]].
 24. ATLAS Collaboration, *Phys. Rev. D* **93**, 092005 (2016), [arXiv:1511.08352 [hep-ex]].
 25. CMS Collaboration, *JHEP* **05** (2014) 104, [arXiv:1401.5041 [hep-ex]].
 26. CMS Collaboration, *JHEP* **06** (2019) 093, [arXiv:1809.03590 [hep-ex]].
 27. ATLAS Collaboration, *Phys. Rev. D* **90**, 112015 (2014), [arXiv:1408.7084 [hep-ex]].
 28. CMS Collaboration, *Eur. Phys. J. C* **74** (2014) 3076, [arxiv:1407.0558 [hep-ex]].
 29. ATLAS Collaboration, ATLAS-CONF-2020-026, https://cds.cern.ch/record/2725727.
 30. CMS Collaboration, *JHEP* **11** (2018) 185, [arXiv:1804.02716 [hep-ex]].
 31. CMS Collaboration, CMS-PAS-HIG-19-015, https://cds.cern.ch/record/2725142.
 32. ATLAS Collaboration, Submitted to EPJC, [arXiv:2004.03447 [hep-ex]].
 33. CMS Collaboration, CMS-PAS-HIG-19-001
 34. A. Hoecker *et al.*, CERN-OPEN-2007-007, [arXiv:physics/0703039 [physics.data-an]].
 35. F. Predregosa *et al.*, *Journal of Machine Learning Research* (2011), [arXiv:1201.0490 [cs.LG]].
 36. D. de Florian *et al.*, CERN-2017-002, [arXiv:1610.07922 [hep-ph]].
 37. S. Badger *et al.*, FERMILAB-CONF-16-175-PPD-T, [arXiv:1605.04692[hep-ph]].
 38. N. Berger *et al.*, LHCHXSWG-2019-003, DESY-19-070, [arXiv:1906.02754[hep-ph]].
 39. S. Amoroso *et al.*, 11th Les Houches Workshop on Physics at TeV Colliders, [arXiv:2003.01700[hep-ph]].
 40. ATLAS Collaboration, [arXiv:2004.03969 [hep-ex]].
 41. ATLAS Collaboration, *JHEP* **10** (2017), 132 [arXiv:1708.02810 [hep-ex]].
 42. ATLAS Collaboration, ATLAS-CONF-2019-029.
 43. ATLAS Collaboration, CMS-PAS-HIG-19-001.
 44. CMS Collaboration, *Phys. Lett. B* **792** (2019), 369-396 [arXiv:1812.06504 [hep-ex]].
 45. CMS Collaboration, *JHEP* **01** (2019), 183 [arXiv:1807.03825 [hep-ex]].
 46. CMS Collaboration, [arXiv:2007.01984 [hep-ex]].
 47. P.A. Zyla *et al.* (Particle Data Group), *Prog. Theor. Exp. Phys.* 2020, 083C01 (2020) <https://doi.org/10.1093/ptep/ptaa104>
 48. H. Baer *et al.*, [arXiv:1306.6352 [hep-ph]].
 49. J. B. Guimarães da Costa *et al.* [CEPC Study Group], [arXiv:1811.10545 [hep-ex]].
 50. A. Abada *et al.* [FCC Collaboration], *Eur. Phys. J. ST* **228**, no. 2, 261 (2019).
 51. J. L. Abelleira Fernandez *et al.* [LHeC Study Group], *J. Phys. G* **39**, 075001 (2012) [arXiv:1206.2913 [physics.acc-ph]].
 52. T. Han and B. Mellado, *Phys. Rev. D* **82**, 016009 (2010) [arXiv:0909.2460 [hep-ph]].

-
53. S. S. Biswal, R. M. Godbole, B. Mellado and S. Raychaudhuri, *Phys. Rev. Lett.* **109**, 261801 (2012) [arXiv:1203.6285 [hep-ph]].
54. P. Agostini *et al.* [LHeC and FCC-he Study Group], [arXiv:2007.14491 [hep-ex]].
55. C. Mosomane, M. Kumar, A. S. Cornell and B. Mellado, *J. Phys. Conf. Ser.* **889**, no. 1, 012004 (2017) [arXiv:1707.05997 [hep-ph]].